Pergamon

Bulletin of Mathematical Biology, Vol. 57, No. 6, pp. 899–929, 1995
Elsevier Science Inc.
Society of Mathematical Biology
Printed in Great Britain.

0092-8240(95)00305-A

THE POTASSIUM A-CURRENT, LOW FIRING RATES AND REBOUND EXCITATION IN HODGKIN–HUXLEY MODELS

■ MAUREEN E. RUSH
Department of Mathematics,
California State University,
Bakersfield, California 93311, U.S.A.

■ JOHN RINZEL
Mathematical Research Branch, NIDDK,
National Institutes of Health,
Bethesda, Maryland 20892, U.S.A.

It is widely believed, following the work of Connor and Stevens (1971, *J. Physiol. Lond.* **214**, 31–53) that the ability to fire action potentials over a wide frequency range, especially down to very low rates, is due to the transient, potassium A-current (I_A). Using a reduction of the classical Hodgkin–Huxley model, we study the effects of I_A on steady firing rate, especially in the near-threshold regime for the onset of firing. A minimum firing rate of zero corresponds to a homoclinic bifurcation of periodic solutions at a critical level of stimulating current. It requires that the membrane's steady-state current–voltage relation be N-shaped rather than monotonic. For experimentally based generic I_A parameters, the model does not fire at arbitrarily low rates, although it can for the more atypical I_A parameters given by Connor and Stevens for the crab axon. When the I_A inactivation rate is slow, we find that the transient potassium current can mediate more complex firing patterns, such as periodic bursting in some parameter regimes. The number of spikes per burst increases as g_A decreases and as inactivation rate decreases. We also study how I_A affects properties of transient voltage responses, such as threshold and firing latency for anodal break excitation. We provide mathematical explanations for several of these dynamic behaviors using bifurcation theory and averaging methods.

1. Introduction.

The Hodgkin–Huxley (1952) equations have been used to describe action potential generation in many excitable cells. In their

Address correspondence to: Dr. John Rinzel, Mathematical Research Branch, NIDDK, National Institutes of Health, BSA Bldg., Suite 350, Bethesda, MD 20892, U.S.A.

original form, they predict repetitive firing for constant applied current over an interval of values. Moreover, the minimum firing frequency is rather high (> 50 Hz). The emergence of stable oscillations with finite amplitude and non-zero frequency is a consequence of the subcritical Hopf bifurcation structure of periodic solutions to the equations (Rinzel, 1978). For neurons which tend to fire at very low rates and which rely on a broad range of frequencies for encoding information, this model does not provide a satisfactory description. Various adjustments to the Hodgkin–Huxley (HH) equations have been made in order to increase the frequency range and to better describe low-frequency firing. These include decreasing the rate of potassium activation in the subthreshold voltage range (Shapiro and Lenherr, 1972; Dodge, 1972) or adding a very slow potassium conductance to a system of equations qualitatively similar to the HH model (Kernell and Sjoholm, 1973). In their study of molluscan nerve somata, Connor and Stevens (1971) attributed low firing rates to the presence of a second potassium current, the transient A-current (I_A). This current, which typically activates rapidly and inactivates more slowly, was subsequently incorporated in an HH-like model (Connor, Walter and McKown, 1977) that fired at rates as low as 2 Hz. It is significant that in their model none of the conductances is particularly slow. Their A-current plays a role at subthreshold voltages to lengthen the interspike interval by working against excitatory input that tends to destabilize the rest state. We show that a necessary condition to obtain arbitrarily low rates of firing is that the membrane's steady-state current–voltage relation be non-monotonic, and that this leads to a different (non-Hopf-like) bifurcation structure for the emergence of periodic behavior.

Transient potassium currents are present in many excitable cells (Rogawski, 1985). This prevalence motivated our comparison of A-current data to determine if and how parameter values for I_A lead to low firing rates in HH-like systems. We have compared these data for I_A while retaining the relationship of their voltage ranges for activation/inactivation to those of the HH-like spike generating currents to arrive at a few representation I_A parameter sets. We study low-frequency firing by using techniques of numerical bifurcation theory, focusing on the onset of stable periodic orbits (a homoclinic bifurcation, in the case of zero minimum frequency), and the dependence of this bifurcation on A-current parameters. We have explored the effects of the maximal conductance for I_A, of the time constant for I_A inactivation and for the voltage range for activating I_A. For the data set we consider most typical, we find that I_A does not lower the firing frequency arbitrarily close to zero. However, the A-current shifts the frequency–current curve to a more depolarized interval of applied current, and so effectively reduces the frequency of firing. In a later section we show by

example how, in contrast to biophysical folklore, low rates can be accomplished with a modified HH model without an A-current. We have also found new firing patterns due to I_A. If the inactivation rate of the A-current is slow, additional bifurcations (period-doubling) emerge along the branch of periodic solutions. Also, periodic bursting occurs, where the number of sodium spikes in a burst depends on the maximal conductance of the A-current. We use the method of averaging to analyze the bursting behavior.

Many cell types that fire repetitively under constant depolarizing stimulation also show the phenomenon of anodal break excitation, as do the Hodgkin–Huxley equations (FitzHugh, 1976). This is a cell's response of one or more action potentials after the end of a sustained hyperpolarizing stimulus. The A-current opposes such rebound behavior since I_A recovers from inactivation during hyperpolarization. Indeed, it can suppress excitation after deep hyperpolarization. In this case, we find that there may be a finite window of hyperpolarization levels from which the cell can fire upon release; the classical HH model has an infinite window. Associated with the rebound response, I_A can cause a prolonged latency, or time to peak, of the action potential. We show that this latency can be foreshortened by appropriately timed stimuli, and this may have consequences for integration of specifically timed synaptic inputs.

For those readers who may have secondary interest in the mathematical details of our findings, in section 3 we briefly summarize our work in biophysical terms with less mathematical depth. The bifurcation structures associated with steady-state, repetitive firing and bursting solutions are described in section 4, while sections 5 and 6 deal with the transient behavior.

2. Hodgkin–Huxley Models and Data for I_A.

2.1. *Models of Connor* et al. The role of the A-current in repetitive firing was first described by Connor and Stevens (1971) for a molluscan neuron. A quantitative description of the A-current was later incorporated by Connor, Walter and McKown (CWM) (1977) in a Hodgkin–Huxley based model for the type-I crab axon. The model's current-balance equation is

$$\dot{V} = -I_{Na} - I_K - I_A - I_L + I_{app},$$

where $I_{Na} = I_{Na}(V, m, h) = \bar{g}_{Na} m^3 h (V - V_{Na})$, $I_K = I_K(V, n) = \bar{g}_K n^4 (V - V_K)$ and $I_A = I_A(V, a, b) = \bar{g}_A a^3 b (V - V_K)$. A constant leakage current $I_L = g_L(V - V_L)$ is also included. The equilibrium potentials V_{Na}, V_K and V_L supply a driving force for the specific conductance. Throughout this paper

we use the units milliseconds for time, millivolts for voltage and microamperes per square centimeter for current, and the values $V_{Na} = 55$ mV, $V_K = -72$ mV and $V_L = -17$ mV. The CWM model consists of the five ordinary differential equations

$$\dot{V} = -g_{Na} m_\infty^3(V) h (V - V_{Na}) - \left[g_K n^4 + g_A a^3 b \right](V - V_K) - I_L(V) + I_{app},$$

where the gating variables satisfy equations of the form

$$\dot{x} = \left(x_\infty(V) - x\right)/\tau_x(V), \qquad x = h, m, n, a, b. \tag{1}$$

Since sodium activation is very rapid, we consider it instantaneous and set $m = m_\infty(V)$. Each of the steady-state functions $x_\infty(V)$ $(x = m, h, n, a, b)$ satisfies the properties $0 < x_\infty(V) < 1$ and $\lim_{V \to -\infty} x_\infty(V) = 0$, $\lim_{V \to \infty} x_\infty(V) = 1$ for activation (m, n, a), while the same limits hold for $1 - x_\infty(V)$ in the case of inactivation (h, b). Notice that there is no inactivation of I_K. In the Appendix we list the Hodgkin–Huxley steady-state gating $x_\infty(V)$ and rate $\tau_x(V)$ functions along with other parameter values. In the CWM model these functions were slightly modified to account for the voltage-clamp data of Connor and Stevens (1971): $x_\infty(V)$ and $\tau_x(V)$ are shifted along the voltage axis by an amount σ_x, $x = m, h, n$ (see the Appendix). The steady-state activation and inactivation functions for the A-current are complicated but satisfy the above properties:

$$a_\infty(V) = \left\{ \frac{0.0761 \exp[(V + 94.22)/31.84]}{1 + \exp[(V + 1.17)/28.93]} \right\}^{1/3}$$

$$b_\infty(V) = \left\{ \frac{1}{1 + \exp[0.069(V + 53.3)]} \right\}^4.$$

The rate functions are

$$\tau_a(V) = 0.3632 + \frac{1.158}{1 + \exp[(V + 55.96)/20.12]}$$

$$\tau_b(V) = 0.124 + \frac{2.678}{1 + \exp[(V + 50.)/16.027]}.$$

We briefly describe the dynamic properties of the CWM model. How the firing frequency is lowered in the CWM model can be explained by considering the steady-state properties of I_A (Fig. 1). The steady-state

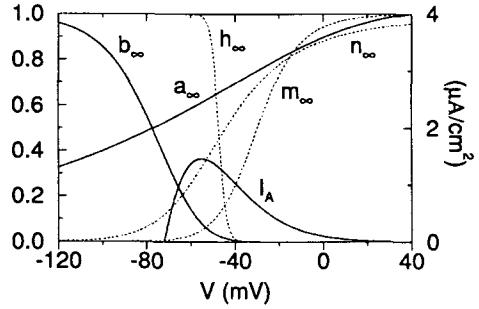

Figure 1. Steady-state gating curves for the ionic currents in the Connor, Walter and McKown (1977) model. The inactivation $b_\infty(V)$ and activation $a_\infty(V)$ curves (solid) for the Connor and Steven's (1971) A-current data show a significant overlap near rest potential (−68 mV). Superimposed steady-state current for I_A (scale on right ordinate). Also shown (dotted) are the steady-state activation curves for I_K and I_{Na} as well as the I_{Na} inactivation curve.

functions $a_\infty(V)$ and $b_\infty(V)$ overlap in a voltage range just below the rest state of the cell (−68 mV). By "overlap" we mean that in some voltage range both gating functions exceed some arbitrary modest value, say 0.1. During the recovery from post-spike hyperpolarization, the two currents I_A and I_L govern V's rate of change. As the voltage depolarizes, I_A activates transiently and slows the voltage increase. This is due to the hyperpolarizing effect of I_A as an outward, potassium current. The total conductance of I_A is then reduced through inactivation, and the membrane voltage slowly approaches threshold for action potential initiation. The A-current continues to inactivate during an action potential, but partially recovers from inactivation during the undershoot (V below rest). This allows for an appreciable amount of I_A in the following interspike interval. An adequate overlap in the $a_\infty(V)$ and $b_\infty(V)$ curves is clearly important. By increasing the maximal conductance g_A, one could totally suppress the rising phase of V and only a steady voltage response would result. So in addition to lowering the frequency, the A-current can shift the I_{app} threshold for onset of repetitive firing. A more detailed analysis of this is given in section 4.

2.2. *A-current data.* The A-current has been quantified for a wide variety of neuronal and non-neuronal cells (Awiszus, 1992; Bargas *et al.*, 1989; Buchholtz *et al.*, 1992; Byrne, 1980; Connor and Stevens, 1971; Connor *et al.*, 1977; Dekin and Getting, 1987; Getting, 1983; Golowasch and Marder, 1992; Graubard and Hartline, 1991; Guckenheimer *et al.*, 1992; Huguenard and McCormick, 1992; Kaczmarek and Strumwasser, 1984; Neher, 1971; McCormick, 1991; Surmeier *et al.*, 1988, 1989; Thompson, 1977, 1982; Williams *et al.*, 1984; also see Rogawski, 1985). A common

feature of these A-currents is that they are inactivated at rest, so no A-current can be elicited unless V is pre-hyperpolarized for a sufficient time to allow recovery from inactivation (i.e. de-inactivation). The most striking variability in the data is the threshold value for activation. In Table 1 we list the gathered data and the steady-state parameters based on the sigmoidal form

$$a_\infty(V) = 1/\left(1 + \exp\left[(V - \theta_a)/k_a\right]\right)$$
$$b_\infty(V) = 1/\left(1 + \exp\left[(V - \theta_b)/k_b\right]\right), \tag{2}$$

where θ_a and θ_b represent voltages at which half-activation or half-inactivation occurs, and $1/(4k_a)$ and $1/(4k_b)$ are the maximum slopes of steady-state activation and inactivation. Table 1 is not exhaustive but reflects the diversity of A-currents in the literature. The table's first column gives the exponent q for activation where I_A is modeled as $g_A a^q b(V - V_K)$. We set $q = 3$ to reflect the data in Table 1. For the purposes of comparison, we relate these data for I_A to a cell's rest state and to the voltage ranges of other active currents (normalization procedure described below). We consider only those data for which I_A is (a) attributed to slowing the frequency of repetitive firing, (b) necessarily contained in a cell with spike generating currents, particularly I_{Na} and I_K, and (c) fully quantified in the literature. These criteria certainly reduce the number of candidates. Nonetheless, variations in the data remain and suggest possible functional roles for I_A.

Table 1. Parameter values for I_A

Activation, a^q			Inactivation, b		
q	θ_a	k_a	θ_b	k_b	References
4	−55	−13.8	−77	7.8	Awiszus (1992)
3	−12	−26	−62	16	Buchholtz *et al.* (1992) Guckenheimer *et al.* (1992)
2	−14	−23	−54	6.5	Byrne (1980)
3	−75	−40	−78	10	Connor *et al.* (1977)
1	−40	−5.5	−68	6.7	Getting (1980)
3	−19.5	−20	−61.5	6	Golowasch and Marder (1992)
3	−35	−10.8	−75	6.5	Guckenheimer *et al.* (1992)
3	−38	−9.8	−63	6.2	Guckenheimer *et al.* (1992)
4	−60	−8	−78	6	Huguenard and McCormick (1992)
4	−36	−20	−78	6.5	Huguenard and McCormick (1992)
3	−42		−65	4	Neher (1971)
	−33	−9	−80	8	Surmeier *et al.* (1988)
	−33	−7.5	−70.5	7.5	Surmeier *et al.* (1989)
	−1.89	−10.8	−47	7	Surmeier *et al.* (1989)

A common feature of I_A is extremely fast activation, so in our analysis we consider it instantaneous by setting $a = a_\infty(V)$ (throughout the paper). In this way, I_A is similiar in time course to the fast sodium current I_{Na}. (Even though τ_a is not as small as τ_m in the CWM model, assuming instantaneous I_A activation has little effect on the results.) On the other hand, the rate of I_A's inactivation varies considerably from cell to cell. For example, τ_b is at least 20 ms according to the data of Huguenard and McCormick (1992) for thalamic neurons (at 36°C), while the rate is as fast as 4 ms in the CWM data at 18.5°C. The rate can be as slow as 1 sec at 10°C (Thompson, 1977); even with an increase in temperature, this is still considered slow. With few exceptions, most of the data indicate that τ_b is independent of voltage. Therefore, we fix τ_b constant and, in our initial analysis, consider τ_b comparable to τ_n (under 2 ms at 18.5°C). Note that although τ_b in the CWM model is voltage-dependent, τ_b is comparable to τ_n. In section 6, we examine the case for τ_b large (above 10 ms).

Our goal is to define a "generic" A-current with properties that represent more of the reported A-currents than the I_A of CWM, which stands apart from the others. We incorporate this current into a reduced version of the standard Hodgkin–Huxley equations (HHA model) and, in the first part of this paper, ascertain whether or not it modulates the firing frequency in the same manner as in the CWM model. To compare the different data sets, we shift the steady-state, half-activation θ_m of I_{Na} to -35 mV, the standard HH value. All other gating functions (for I_K and I_A) are shifted by the same amount, thus maintaining the relative voltage ranges and, certainly, maintaining the overlap in steady-state activation and inactivation for I_A. Aside from the parameter g_A, we specify the parameter vector $(\theta_a, k_a, \theta_b, k_b)$ for each I_A. The CWM data are represented by $(-80, -40, -83, 10)$. From the normalized gating data in Table 2 we see that the crab-axon data differ considerably, with a much shallower and left-shifted activation function. We define as a "generic" parameter set $A_G = (-55, -20, -70, 6)$ wherein the choice of $\theta_a = -55$ reflects a best case, steady-state analysis.

In the previous section, we described how the considerable overlap in $a_\infty(V)$ and $b_\infty(V)$ contributed to I_A's ability to lower the frequency of firing. Yet most of these data sets show a negligible amount of overlap, thereby questioning the contribution of I_A during interspike intervals of steady-firing. As representative of the CWM data we use $A_C = (-75, -50, -70, 6)$ in our analysis of frequency modulation and show which dynamical features persist as θ_a is increased. In an effort to reduce the number of parameters in the analysis, we fix $\theta_b = -70$ and $k_b = 6$.

2.3. *HHA Model.* The CWM model is often used as a paradigm for I_A-mediated low-frequency firing, yet the characteristics of its A-current

Table 2. Selected parameter values for I_A from Table 1, normalized with respect to $\theta_m = -35$ mV, in sodium half-activation value. The last two rows contain the parameter sets in our study

Activation, a^q			Inactivation, b		I_{Na}		I_K	
q	θ_a	k_a	θ_b	k_b	θ_m	θ_h	θ_n	Reference
4	−45	−13.8	−67	7.8	−35	−62	8.3	Awiszus (1992)
3	−39	−26	−89	6	−35	−74	−52	Buchholtz *et al.* (1992)
2	−41	−23	−81	6.5	−35	−44	−21	Byrne (1980)
3	−80	−40	−83	10	−35	−51	−49	Conner *et al.* (1977)
3	−25	−26	−75	16	−35	−54	−31	Guckenheimer *et al.* (1992)
4	−55	−8	−73	6	−35	−63	−30	Huguenard and McCormick (1992)
4	−31	−20	−73	6.5	−35	−63	−30	Huguenard and McCormick (1992)
				Representative parameter sets				
3	−75	−50	−70	−6	−35	−55	−50	A_C
3	−55	−20	−70	−6	−35	−55	−50	A_G

activation data are outlying. We consider whether or not a more "generic" A-current can function in the same role. The dynamical properties of the four-variable Hodgkin–Huxley model are well known. We consider a reduced system of equations with a linear relationship between I_{Na} inactivation and I_K activation, $h + 1.2n = 0.9$ (e.g., Rinzel, 1985). This retains the bifurcation structure of the full system and reduces it to two dimensions. It also exhibits the property of rebound excitation; that is, release from hyperpolarization can result in a single, transient action potential. This behavior is considered in section 5 and 6. Incorporation of I_A adds a third equation for inactivation b. The HHA model is then composed of the following equations:

$$\begin{aligned} \dot{V} &= -g_{Na} m_\infty^3(V)[0.9 - 1.2n](V - V_{Na}) \\ &\quad - \left[g_K n^4 + g_A a_\infty^3(V) b\right](V - V_K) - I_L(V) + I_{app} \\ \dot{n} &= \phi\left(n_\infty(V) - n\right)/\tau_n(V) \\ \dot{b} &= \phi\left(b_\infty(V) - b\right)/\tau_b, \end{aligned} \tag{3}$$

where g_A, τ_b, I_{app} and ϕ are parameters that we vary (ϕ is a temperature feature factor and is discussed later in the paper). The functions $a_\infty(V)$ and $b_\infty(V)$ are given by equations (2). We analyze both steady and transient response properties of the HHA model. In both situations we consider separately the cases of fast and slow inactivation. We fix $\theta_b = -70$ and $k_b = 6$ and only in the case of repetitive firing do we examine the CWM-like

parameters A_C. All other analyses are based on the generic parameter set A_G. The results that follow also hold for the full HH system; however, in some cases the analysis is more tractable in the reduced system.

3. Summary of Results. In this section we provide a brief overview of our findings on the modulatory effects of the A-current on the HHA model's dynamic behavior. We begin by considering the steady firing properties in response to steady current. For the A_C parameter set, our model's frequency range is extended to low rates as g_A increases (see Fig. 4B, but disregard the dashed portions of curves; they correspond to unstable behavior.) The frequency–current relation also shifts rightward with g_A, reflecting the additional depolarizing current needed to overcome the hyperpolarizing effect of I_A. This model thus behaves similarly to the CWM model. The low-frequency behavior develops as the membrane's steady-state current–voltage relation $I_{SS}(V)$ becomes sufficiently N-shaped (seen as the curves in Fig. 3, left). The mathematical limit for very low-frequency firing is an oscillation with infinite period (zero frequency) that appears precisely at the critical current level where $I_{SS}(V)$ has zero slope. Here, the depolarized resting voltage coalesces with a saddle-point threshold voltage. Mathematically, for I_{app} just above criticality, the oscillating system's trajectory in phase space passes through a "subthreshold" region where the velocity is very low. Just a moderate change in g_A can create in this region a stable rest point and a saddle point and cause the system to cease firing repetitively. Thus, as Connor and Stevens (1971) noted, even though no currents have slow gating kinetics, this membrane model can fire at very low rates. In section 4.2 we show that this zero-frequency criticality separates steady-state behavior from low-frequency firing in the (I_{app}, g_A) parameter space.

Figure 6 illustrates the repetitive firing behavior of the HHA model with the A_G parameter set. In this case also, the current–frequency curve shifts rightward as g_A increases (disregard dashed curves). The shift is on the order of the steady-state A-current near the resting voltage regime (about 10 $\mu A/cm^2$ with $g_A = 50.0$ mS/cm^2). However, arbitrarily low firing frequency is not found for the A_G parameter settings. With I_{app} fixed, the frequency is reduced as g_A increases, but this reduction is attributed to the rightward shift in current threshold only (see time courses). The dynamics are qualitatively similar to the standard HH model: stable periodic behavior emerges with non-zero minimum frequency and large amplitude. Thus, while an A-current is not sufficient to give low-frequency firing, neither is it necessary. Indeed, one can adjust the parameters of the standard HH equations, without adding I_A or other currents, to achieve low-frequency firing. In section 4.4 we reduce g_K so that the sodium current I_{Na} domi-

nates in the voltage region just above rest and forms the necessary voltage extrema in the $I_{SS}(V)$ curve. As a result, the frequency response is lowered and zero-frequency firing emerges (Fig. 10, left).

Although our generic A-current, with τ_b comparable to I_K's activation time constant, does not enlarge the HHA model's frequency range to include arbitrarily low rates, other interesting behavior emerges with τ_b larger. With slower I_A inactivation (say, $\tau_b = 10$ ms), complex periodic spiking patterns emerge; high-frequency tonic firing gives way to repetitive bursting of action potentials (Fig. 7, lower). As g_A increases, the number of spikes in a burst decreases, leading eventually to a single-spike burst with a very low spike rate (Fig. 7d). As τ_b is further increased, burst duration and interburst interval both increase; I_A inactivation becomes the slow variable that determines the burst's time scale (Fig. 8, upper left, where $\tau_b = 30$ ms).

We also consider the transient properties of the HHA model (A_G parameter set) in response to a step I_{app} from a hyperpolarized level (Fig. 11). The A-current de-inactivates (b increases) during a hyperpolarized conditioning phase, and then activates transiently when a depolarizing current step is applied. The I_A conductance during activation might be approximated by either $g_A a_\infty^3(V)b$ or $g_A a_\infty^3(V)b_\infty(V)$, depending on the rate of inactivation τ_b^{-1}. If I_{app} exceeds rheobase (the threshold current for repetitive firing) then, in the case of fast inactivation, the initial latency is comparable to the interspike interval of repetitive firing. For slow inactivation, the latency is prolonged, even for relatively small g_A. This delay phenomenon may provide a mechanism to ensure that a neuron fires only in response to a sustained depolarizing input, or to a long enough train of brief stimuli. Moreover, we find that a single brief excitatory pulse after a minimal time into the latent period can advance the onset of firing.

In section 6 we consider the special case of rebound firing upon release from hyperpolarization to $I_{app} = 0$ (anodal break excitation). We find, for fast inactivation, that increasing g_A shifts the anodal rheobase (threshold holding potential for generating a single rebound action potential) in the hyperpolarizing direction (Fig. 13A). That is, the larger is I_A, the more one must de-inactivate I_{Na} and deactivate I_K by pre-hyperpolarization in order to generate an action potential. The effect is similar to that caused by increasing temperature in the standard HH model (FitzHugh, 1976). The rheobase is also lowered in the case of τ_b large. Moreover, a second rheobase (a lower one) is found *below* which no rebound response occurs (Fig. 13B). These two thresholds create a window for rebound excitation which is then modulated by increases in g_A: the I_K-associated (upper) threshold is lowered, as mentioned above, while the lower threshold (directly associated with I_A) is raised (Fig. 13C). This leads to a critical g_A above which no anodal break excitation is possible.

4. Bifurcation Analysis. In this section we analyze the bifurcations that arise in the steady response properties of the CWM and the HHA models. In particular, for the HHA model we indicate the dependence of the steady-state I–V relation on θ_a and k_a. If g_A is sufficiently large, the N-shape of the I–V relation leads to zero-frequency firing in the HHA model. This critical g_A level exceeds biophysically reasonable values in the case of generic parameters. We also consider bifurcations along the periodic branch for τ_b large. We project the voltage trajectory into a phase plane and show how bursts of action potentials arise. For fixed I_{app} the frequency of periodic bursting decreases as g_A increases, and bursting behavior terminates with non-zero burst frequency at a Hopf-bifurcation. We also indicate how other bifurcations occur along the periodic branch by analyzing a one-dimensional averaged system for the dynamics of b.

4.1. *CWM model.* A family of periodic solutions of this model can be represented by a bifurcation diagram in which each periodic solution is associated with a given current stimulus. We use the software package AUTO (Doedel, 1981) to compute the bifurcation diagrams and to produce frequency curves as a function of I_{app}. The fixed points of system (1) are resolved by setting $x = x_\infty(V)$ for all conductances and by letting $\dot{V} = 0$. This defines a steady-state, current–voltage (I–V) relation for the cell

$$\begin{aligned} I_{app} &= I_{SS}(V) \\ &\equiv I_{Na}\big(V, m_\infty(V), 0.9 - 1.2n_\infty(V)\big) \\ &\quad + I_K\big(V, n_\infty(V)\big) + I_A\big(V, a_\infty(V), b_\infty(V)\big) + I_L(V). \end{aligned}$$

The CWM bifurcation diagram of Fig. 2 is computed for a temperature of 18.5°C and with a maximal conductance $g_A = 33$ mS/cm^2 for I_A. The standard value (used by Connor *et al.*, 1977) for g_A is 47.7 mS/cm^2, but we choose a lower value for initial comparison to the Hodgkin–Huxley voltage characteristics. As for the standard HH model, there is an I_{app} interval in which the fixed point is unstable, and this interval is bounded by two Hopf bifurcation points. From the left bifurcation point emerges a branch of unstable periodic solution (open circles). These solutions stabilize at a saddle-node bifurcation on the periodic branch and represent stable repetitive firing (filled circles) until they shrink to zero amplitude at the right Hopf bifurcation point. Since we are interested in the onset of stable periodic behavior as I_{app} is increased from zero, we focus on a region near the left bifurcation only. The inset of Fig. 2 shows firing frequency versus I_{app}; minimum frequency is 9 Hz for this value of g_A. We note that the

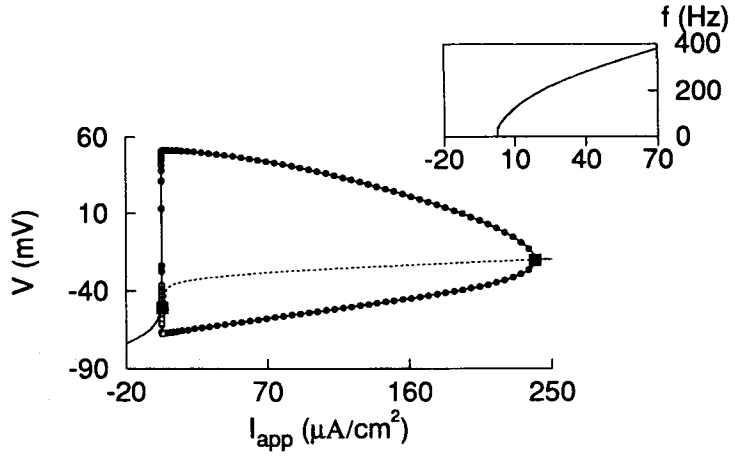

Figure 2. Bifurcation diagram (V vs I_{app}) for the CWM model with $g_A = 33$ mS/cm^2 shows two Hopf bifurcation points (solid squares) on the curve $I_{SS}(V)$ from which periodic solutions emerge (maximum and minimum voltage are plotted as circles: open circles, unstable; filled circles, stable). Top graph shows the firing frequency vs I_{app} for $I_{app} \leq 70$ μA/cm^2.

minimum firing frequency in the CWM model (1) without I_A is approximately 25 Hz.

The bifurcation structure for the CWM model differs from the HH system in the shape of its $I_{SS}(V)$ curve. It was originally observed by Connor *et al.* (1977) that the I–V relation was "flat" in a voltage region near the threshold for repetitive firing. Figure 3 (upper left) compared the $I_{SS}(V)$ curve of CWM for $g_A = 0$ with that of the standard HH. While the $I_{SS}(V)$ curve for both cases is monotone, the curve of the CWM model is close to degenerate. As g_A is increased (left panels of Fig. 3), a pair of saddle-node points emerges and, for g_A approximately 47.82 mS/cm^2, the left saddle-node contacts the branch of periodic solutions. At this point of contact an unstable homoclinic orbit is formed. Voltage time courses in the right panel of Fig. 3 are measured at $I_{app} = 10$ μA/cm^2. The lowered firing frequency ($g_A = 50$ mS/cm^2) is attributed to the close proximity in I_{app} of stable periodic solutions to the homoclinic orbit. In fact, with further increases in g_A ($g_A = 60$ mS/cm^2), the homoclinic orbit becomes stable and large amplitude, zero-frequency firing is possible.

4.2. *Zero-frequency onset in HHA.* We consider the HHA model (3) with the associated steady-state I–V relation given by

$$I_{SS}(V) = I_{Na}(V, 0.m_\infty(V), 9 - 1.2n_\infty(V)) + I_K(V, n_\infty(V)) + I_A(V, a_\infty(V), b_\infty(V)) + I_L(V)$$

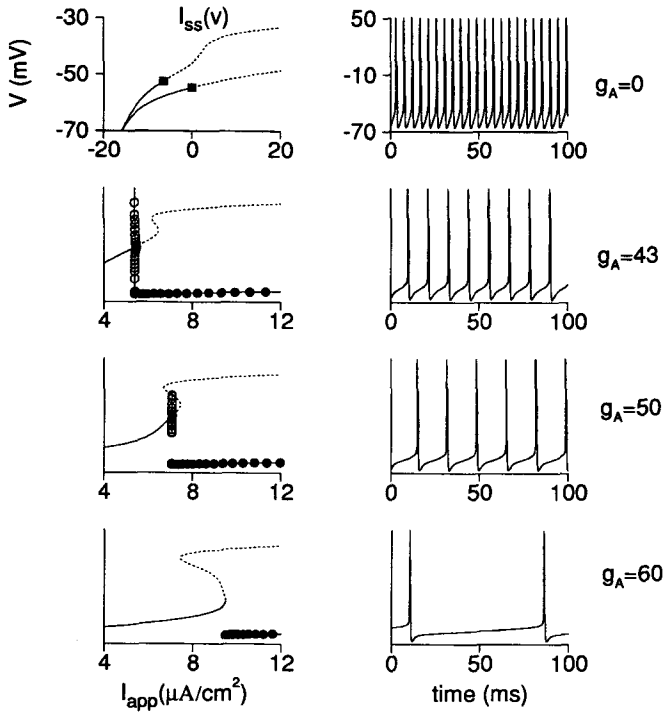

Figure 3. Steady behavior of the CWM model as a function of I_{app} for four values of g_A ($\tau_b = 1$ ms). Left panels: Bifurcation diagrams for steady-state and periodic solutions; same plotting symbols as in Fig. 2, except maximum V for oscillations is off-scale (not shown). Right panels: Voltage time courses for $I_{app} = 10$ μA/cm^2. For $g_A = 0$, the steady-state $I_{SS}(V)$ curve is monotonic (upper) as in the standard HH model (lower). Both models have onset of repetitive firing via subcritical Hopf bifurcation (not shown). For $g_A =$ 43 mS/cm^2 emergence of periodic behavior remains via subcritical Hopf bifurcation (as in Fig. 2), but the $I_{SS}(V)$ curve has developed extrema; two saddle-node fixed points are found. For $g_A = 50$ mS/cm^2 the branch of unstable periodic solutions terminates on the middle (saddle) branch of $I_{SS}(V)$ in a homoclinic orbit. This periodic branch disappears as g_A increases and the extrema move further apart. For $g_A = 60$ mS/cm^2 the stable periodic solutions to the right terminate in a homoclinic orbit at the saddle-node fixed point. Note that time courses show considerable reduction in firing frequency as g_A is increased.

or

$$I_{SS}(V; g_A) = I_{HH}(V) + I_A(V; g_A). \tag{4}$$

For A_C parameters, the bifurcations which arise as g_A is increased are those described previously for the CWM model. Saddle-node bifurcations are found by setting the derivative of (4) equal to zero. The steady-state curve $I_{HH}(V)$ is monotone increasing, so existence of saddle-node points

depends on the voltage range in which I_A decreases. For $V > V_K$ define the functions

$$F^+(V) = \frac{3}{|k_a|}\left[1 - a_\infty(V)\right] b_\infty(V)(V - V_K) + b_\infty(V)$$

$$F^-(V) = b'_\infty(V)(V - V_K). \tag{5}$$

Then $I'_A(V; g_A) = g_A a_\infty^3(V)\{F^+(V) + F^-(V)\}$, where $F^+(V) \geq 0$ and $F^-(V) \leq 0$. For fixed $g_A > 0$, if V^* is the point at which $I'_A = 0$, then we have $|F^-(V)| > F^+(V)$ for $V > V^*$. Notice that the term $F^+(V)$ is reduced for $|k_a|$ large or if $a_\infty(V) \approx 1$; depending on the parameters k_a and θ_a, I'_A can equal zero at a lower voltage. In particular, $I'_A(V^*; g_A) = 0$ for $g_A > 0$ and V^* in a voltage region where $I'_{HH}(V)$ is small. Given the A_C data $\theta_a = -75$ and $k_a = -50$, one can show that $I'_{SS}(V; g_A) = 0$ for V near V^* and $g_A > 0$. Since I_A is an outward current, the I_{app} value at which the saddle-node bifurcation occurs increases with g_A.

Figure 4A shows two curves of saddle-node (SN) bifurcation points originating from a cusp point in (I_{app}, g_A) parameter space. For fixed g_A below this cusp point, the vector field of HHA is qualitatively similar to the standard HH system: there is a Hopf bifurcation point (HB) and, to the left, a saddle-node bifurcation on the periodic branch (SNP), the point at which a stable and an unstable periodic solution coalesce. The region of stable periodic firing is then to the right of the SNP curve. This curve is continued numerically in (I_{app}, g_A) space using AUTO and terminates generically at a codimension 2, global bifurcation with a homoclinic (saddle-loop) orbit (beginning of thick solid curve in Fig. 4A). Recall in the CWM model (Fig. 3; $g_A = 50$ mS/cm^2) that a homoclinic orbit is present between the saddle-node points. The situation is similar here. To see this, fix $g_A = 135$ mS/cm^2 in Fig. 4A and consider the bifurcation structure as I_{app} is increased (horizontal line). Between the saddle-node bifurcation points, the system has three fixed points. The subcritical branch of periodic orbits from HB terminates at a saddle fixed point and forms an unstable homoclinic orbit (dotted curve HC1) to the left of the HB point. Moreover, a second, stable homoclinic orbit is coincident with the right saddle-node fixed point (thick curve HC2). It is this curve of homoclinic orbits on which the SNP curve terminates. It follows that the region of stable periodic solutions (shaded) is bounded on the left by the curves SNP and HC2, and as g_A increases from zero, the minimum frequency can go to zero.

The stable homoclinic orbit persists for larger values of g_A, although the unstable homoclinic orbit (HC1) disappears in a Takens–Bogdanov bifurcation (TB point; Takens, 1974; Bogdanov, 1975). In Fig. 4B we plot the

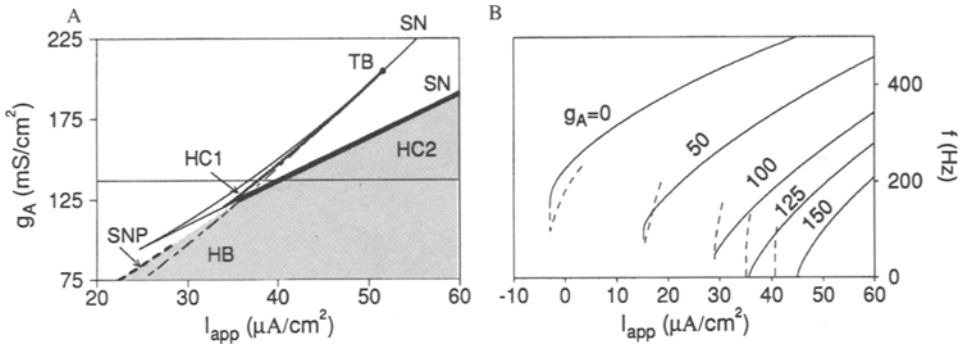

Figure 4. (A) Two-parameter (I_{app}, g_A) response diagram for the HHA model with A_C parameter set and $\tau_b = 1$ ms. The region of stable periodic solutions is shaded. For $g_A = 75$ mS/cm^2 the bifurcation structure as a function of I_{app} is as in Fig. 2: stable periodic solutions emerge from a saddle-node bifurcation on the periodic solution branch SNP (dashed). The system is bistable between SNP and HB (mixed dashes), the left Hopf bifurcation point in HHA. As g_A increases, two saddle-node fixed point curves SN (solid) emerge from a cusp point; inside this cusp, the HHA system has three fixed points (node, saddle, unstable spiral). For $g_A = 135$ mS/cm^2 (horizontal line) the HB point is inside the cusp region, and the unstable periodic solutions which emerge from it terminate with infinite period at HC1 (dotted). HC1 and HB curves intersect at TB, a Takens–Bogdanov bifurcation. The stable periodic solutions (for $g_A \geq 125$ mS/cm^2) terminate in a homoclinic orbit HC2 single curve. (B) Firing frequency versus current curves for the HHA model with A_C parameter set and $\tau_b = 1$ ms. Without I_A the minimum frequency is approximately 100 Hz. As g_A increases, the threshold current for repetitive firing increases. With A_C parameters, the frequency range is increased as both the unstable and stable periodic solutions approach zero-frequency onset as g_A is increased. Notice that the region of bistability shrinks as HB (endpoint of unstable frequencies) and SNP (the turning point for stable frequencies) converge and the continuous solution branch splits into two distinct branches.

frequency–current (f–I) curves as a function of g_A for the parameter set $A_C = (-75, -50, -70, 6)$. If we measure the frequency for a fixed I_{app} level, say $I_{app} = 40$ μA/cm^2, then increases in g_A reduce the frequency arbitrarily close to zero. With an understanding of the above two-parameter bifurcation schemes, we can now consider easily what happens in the HHA model when θ_a is increased from -75 to -55. This information is presented in the (I_{app}, θ_a) parameter space in Fig. 5 computed for $g_A = 125$ mS/cm^2. The bifurcation scheme reverses itself: As θ_a increases, both homoclinic orbits disappear, and the only remaining periodic solutions are those to the right of the SNP curve. Moreover, the overlap of $a_\infty(V)$ with $b_\infty(V)$ is not sufficient for a non-monotone $I_{SS}(V)$ curve. For $\theta_a = -55$ the minimum frequency occurs at SNP and equals 61.8 Hz, closer to the standard HH level. However, the Hopf bifurcation point is still affected by

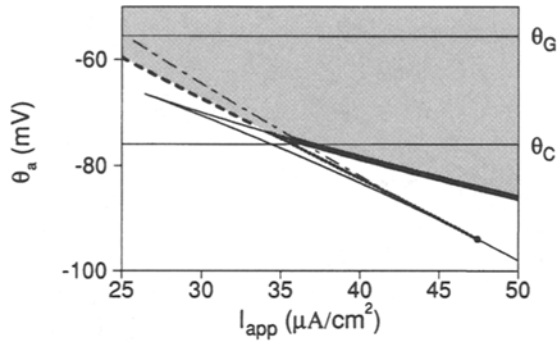

Figure 5. Two parameter (I_{app}, θ_a) response diagram for $g_A = 125$ mS/cm^2 in the HHA model with A_C parameter set and $\tau_b = 1$ ms shows the effect of shifting $a_\infty(V)$ upward along the voltage axis. Symbol convention as in Fig. 4A. The emergence of zero-frequency firing (HC2) requires low voltage activation, θ_a below the A_C value. For high voltage activation, periodic solutions emerge with non-zero frequency from SNP, the saddle-node bifurcation on the periodic branch.

the presence of I_A, even with k_a adjusted to -20. This in itself has consequences for the firing frequency. As shown by the voltage time courses in Fig. 6, if we fix $I_{app} = 40$ μA/cm^2 with parameters $A_G = (-55, -20, -70, 6)$ and increase g_A, the frequency is indeed lowered. Yet, for the generic parameters, the range of frequencies for steady firing is

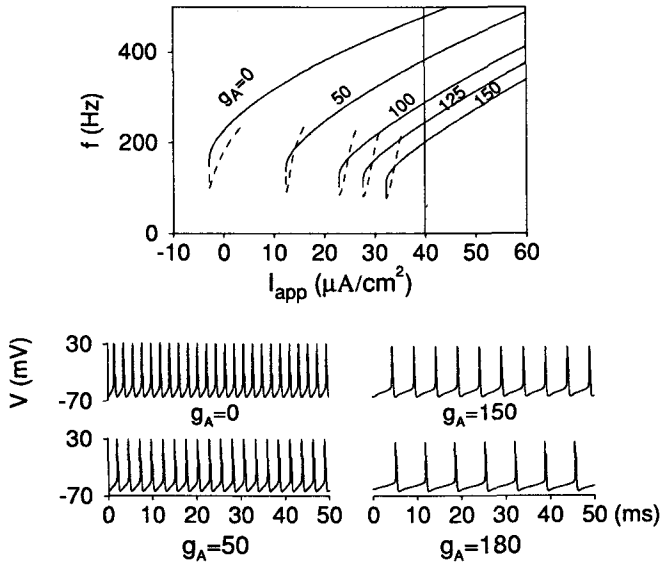

Figure 6. Frequency–current for the HHA model with A_G parameter set and $\tau_b = 1$ ms. Increasing g_A increases the rheobase, but the minimum firing frequency is not reduced to zero. V time courses for $I_{app} = 40$ μA/cm^2 indicate a reduction in frequency as g_A is increased.

hardly affected. Increasing g_A shifts the HB point to larger I_{app} values and lowers only slightly the range of frequencies for steady firing. Our analysis suggests that the I_A we identify as generic has a more quantitative than qualitative role in modulating the frequency of repetitive firing. Based on this, we conjecture that the A-current may reduce the frequency to zero if the spike generating system (e.g. HH-like model with $I_A = 0$) has the propensity toward low-frequency firing. In section 4.3 we give an example of a modified HH system in which zero-frequency firing without an A-current is possible.

4.3. *Periodic branch bifurcations and bursting.* We have shown that generic I_A data shift the frequency–current curve to a more depolarized I_{app} interval. This is also the case for τ_b large, although this shift is not uniform. For example, compare the frequency curves for $g_A = 0$ and $g_A = 50$ mS/cm^2 in Fig. 7. For $g_A = 0$ there is an I_{app} interval between SNP and the Hopf bifurcation in which both the fixed point and the periodic solutions are stable. For $g_A = 50$ mS/cm^2 there is no longer this region of bistability. Moreover, there is an I_{app} interval in which both the fixed point

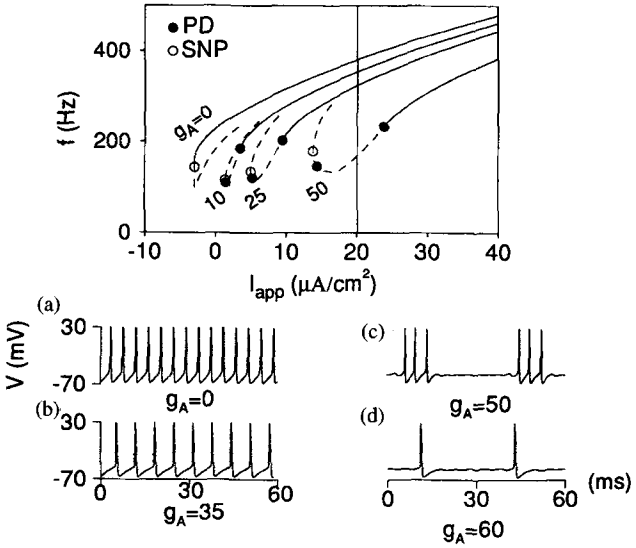

Figure 7. Frequency–current curves (upper panel) for HHA model with A_G parameter set and $\tau_b = 10$ ms. Increased g_A shifts the curves rightward in I_{app} and the slower rate of inactivation τ_b^{-1} creates additional bifurcations (PD—period doubling) along the branch of periodic solutions. Time courses to repetitive behavior for $I_{app} = 20$ μA/cm^2 are shown in the lower panel. As g_A increases, the frequency is reduced slightly until the behavior changes qualitatively at the PD (subcritical) point. Periodic bursting of action potential emerges with low frequency ($g_A = 50$ mS/cm^2). As g_A increases, the number of action potential in a burst decreases (1 spike per burst for $g_A = 60$ mS/cm^2).

and periodic branch are unstable. This interval is bounded on the left by the Hopf bifurcation and on the right by a period-doubling bifurcation (rightmost PD). In this interval, stable complex firing patterns are found. Awiszus (1992) has recently reported action potential "doublets" during a constant excitatory input to a HH-like model with an A-current. In our case the period-doubled solutions are unstable. Here, we find that stable repetitive firing is replaced by periodic bursts of action potentials. This transition is illustrated by the time courses in Fig. 7 for $I_{app} = 20\ \mu A/cm^2$ as g_A is increased. Intuitively, a burst occurs because I_A slowly de-inactivates (b increases) during repetitive firing to eventually inhibit firing. The voltage is then quiescent with I_A contributing to the stability of a temporary resting state. During this phase, I_A slowly inactivates (b decreases) and firing resumes as the rest point destabilizes. The cycle then repeats, resulting in periodic bursts of action potentials.

In order to examine the emergent dynamics, particularly the frequency of bursting and its dependence on g_A, we define the variable $b_A = g_A b$, which, for large τ_b, changes slowly compared to V and n. The HHA system is then written as

$$\begin{aligned} \dot{V} &= -I_{Na}(V, m_\infty(V), n) - I_K(V, n) - I_A(V, a_\infty(V), b_A) - I_L(V) + I_{app} \\ \dot{n} &= (n_\infty(V) - n)/\tau_n(V) \\ \dot{b}_A &= (g_A b_\infty(V) - b_A)/\tau_b. \end{aligned} \tag{6}$$

This is a convenient formulation since modulations in g_A affect only the slow dynamics. If we fix $I_{app} = 20\ \mu A/cm^2$, then for $g_A = 0$, the repetitive firing behavior of the model converges to a stable periodic solution on the periodic branch; this is a solution of the fast subsystem of (6) given by the equations for V and n. To illustrate the dependence of the fast subsystem on b_A (in the limit as $\tau_b \to \infty$), we plot in Fig. 8B the bifurcation structure of the (V, n) subsystem with respect to the parameter b_A. There is a subcritical Hopf bifurcation at $b_A = b_{HB}$ and stable periodic solutions are found for $0 \le b_A < b_P$, where b_P is the turning point in the periodic branch. The nature of the Hopf bifurcation provides a classical situation in which periodic bursting is found: hysteresis, or bistability, in the fast subsystem (Rinzel, 1987). A bursting solution is viewed as an orbit which alternates between the branch of stable periodic solutions (firing phase) and the steady-state branch (silent phase). The flow is determined by the time, on average, that the orbit is either above or below the surface defined by $\dot{b}_A = 0$. In Fig. 8B we show the projection of the bursting solution of Fig. 8A ($g_A = 50\ mS/cm^2$ and $\tau_b = 30$ ms) into the (V, b_A) phase plane. Due

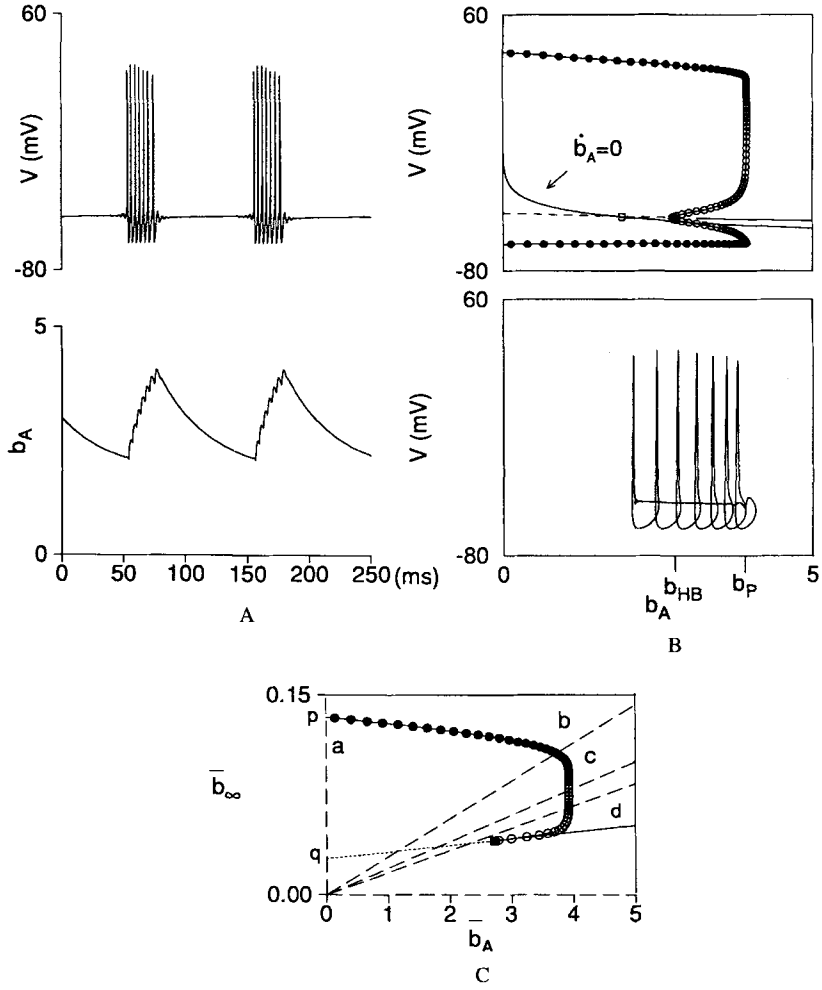

Figure 8. Analysis of periodic bursting mediated by a slowly inactivating I_A. (A) Voltage time course of a bursting solution (with b_A's time course shown below) for $I_{app} = 20$ μA/cm^2 with $g_A = 50$ mS/cm^2 and $\tau_b = 30$ ms. (B) The fast subsystem's bifurcation diagram with b_A as control parameter; here, $b_A = g_A b$ (see equation (6)) and $I_{app} = 20$ μA/cm^2. Unstable periodic solutions (open circles) emerge via Hopf bifurcation at $b_A = b_{HB}$ and connect continuously at $b_A = b_P$ with stable periodic solutions (filled circles). The slow null surface $\dot{b}_A = 0$ intersects the steady-state curve of the fast subsystem at an unstable fixed point (open square). It also intersects the branch of periodic solutions at $b_A = 0$ (stable branch) and for b_A inside the bistable region (b_{HB}, b_P) (unstable branch). Trajectory of bursting solution from (A) is projected (below) here as V versus b_A. (C) Fixed points of the averaged equation (8) occur when the line with slope $1/g_A$ intersects the curve $\bar{b}_\infty$ versus b_A; four cases, a–d, shown here correspond to those in Fig. 7. A fixed point that lies on the filled circle curve corresponds to stable repetitive firing (cases a and b). For cases c and d, repetitive firing is unstable; periodic bursting is the stable response. Each fixed point on the dotted curve corresponds to an unstable fixed point of the full system.

primarily to the hyperpolarizing portion of each action potential, there is an average increase in inactivation b_A, and firing terminates when the orbit falls from the periodic branch near $b_A = b_P$. During the silent phase, b_A inactivates along the steady-state branch for the fast subsystem. Moreover, there is "ramp" effect (Baer *et al.*, 1989): the orbit flows leftward past the bifurcation point at b_{HB}, remaining for a finite time in a neighborhood of the unstable branch of the fast subsystem. Under the assumption that the rate of b_A is uniform in the silent phase, the orbit travels an approximately equal distance on either side of the Hopf bifurcation. The active phase is then initiated at approximately $b_A = 2b_{HB} - b_P$. The flow is once again rightward, and the cycle repeats.

The fast subsystem of the HHA system is independent of g_A, and so for modulations in g_A the same bifurcation diagram holds, but the slow null-surface changes: half-inactivation is at $V = -70$ mV and $b_A = g_A/2$. It follows that the unstable fixed point of the full system approaches b_{HB} as g_A increases. The active phase is initiated for higher values of b_A and, as a consequence, the number of action potentials in a burst is fewer. The active phase is shorter, but surprisingly, the silent phase is not. What is interesting to note here is that, although there is less distance to traverse in b_A, the orbit slows down considerably as it approaches the fixed point of the full system. As a result, the number of spikes in a burst is decreased, *and* the burst frequency is decreased (see Fig. 9). The assumption here is that g_A does not affect the rate of flow in the active phase, while it is clear that the rate at which b_A decreases is controlled by g_A.

We conclude this section by discussing the bifurcations that we found using AUTO. For $\tau_b = 10$ ms the frequency curve (Fig. 7) indicates period-doubling bifurcations (filled circles) and a saddle-node bifurcation on the

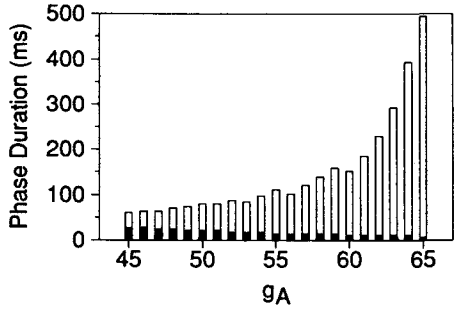

Figure 9. Duration in the silent phase (open bars) and active phase (filled bars) for the type of bursting solution shown in Fig. 8A, as a function of g_A with $\tau_b = 30$ ms. Burst frequency decreases as the trajectory spends more time in the silent phase. The reduced time in the active phase necessarily decreases the number of action potentials in a burst.

periodic branch (open circle). To understand which bifurcations are expected to appear in the limit of large τ_b we consider the averaged dynamics of b_A. In equation (6) we can replace $b_\infty(V)$ by its average over the voltage activity $V(t; b_A)$ given by the fast subsystem of (6) with b_A treated as a parameter. For a periodic solution $V(t; b_A)$ of the fast subsystem this average is defined as

$$\bar{b}_\infty(b_A) = \frac{1}{T}\int_0^T b_\infty(V(t; b_A))\,dt, \tag{7}$$

where T is the oscillation period. If $V = V_{SS}(b_A)$ is a steady-state (time-independent) solution, then $\bar{b}_\infty(b_A) = b_\infty(V_{SS}(b_A))$. This averaging procedure reduces our three-variable system to a one-variable description:

$$\dot{\bar{b}}_A = \left[g_A \bar{b}_\infty(\bar{b}_A) - \bar{b}_A\right]/\tau_b. \tag{8}$$

This equation describes the average inactivation $\bar{b}_A$ of I_A. While numerically computing $V(t; b_A)$ for the bifurcation diagram of Fig. 8B, we evaluate $\bar{b}_\infty(\bar{b}_A)$ from (7). In Fig. 8C we plot the resultant curve $\bar{b}_\infty(\bar{b}_A)$, where we indicate the stability inherited from the fast subsystem. A fixed point of (8) satisfies $\bar{b}_\infty(\bar{b}_A) = (1/g_A)\bar{b}_A$ and corresponds, under certain conditions, to periodic solutions of the full system. For example, for $g_A = 0$ (vertical axis in Fig. 8C) there are two fixed points p and q. The point q corresponds to the unstable fixed point of the full system, while p corresponds to the periodic orbit of the full system. This periodic orbit is stable if p is a stable fixed point of (8). Note that the lines a–d in Fig. 8C correspond to the time courses a–d in Fig. 7. As g_A increases, p remains stable as long as it intersects the "stable" portion of $\bar{b}_\infty(\bar{b}_A)$; this is not obvious from the figure since the slope of $\bar{b}_\infty(\bar{b}_A)$ is so severe. However, as the line $(1/g_A)\bar{b}_A$ passes over the limit point of the fast subsystem, the stability of the fixed point p changes. When the full system is analyzed, we find numerically that two complex-valued Floquet multipliers cross the unit circle simultaneously for $g_A = 45.19$ mS/cm^2 and $\tau_b = 100$ ms. This corresponds to a Hopf bifurcation on the periodic branch rather than the period-doubling bifurcations that were found for $\tau_b = 10$ ms. For further increases in g_A, the fixed point q stabilizes by undergoing a Hopf bifurcation (at $g_A = 66.97$ mS/cm^2), and the periodic bursting solutions terminate. Beyond the Hopf bifurcation, there are three fixed points to the averaged system: the stable fixed point q and two unstable points, each corresponding to unstable periodic solutions of the full system. For $g_A = 79.24$ mS/cm^2 the two unstable fixed points disappear in a saddle-node bifurcation. This corresponds to the saddle-node bifurcation on the periodic branch of the full system.

4.4. *HH example for zero-frequency firing.* We conclude this section with an example of an HH system in which zero-frequency firing is possible without an A-current. There are many adjustments to the standard HH equations which can change its bifurcation structure (Hassard and Shiau, 1991; Labouriau, 1989; Rinzel, 1979). Here we shift I_{Na} inactivation rightward by 7 mV to create a greater window current for I_{Na}. Together with a shift leftward by 1 mV in I_K activation, reductions in g_K allow for a greater contribution of I_{Na}. As a result, the I–V relation has a negative slope region (N-shaped). (We note that the CWM model without I_A also gives zero-frequency firing for g_K reduced to 10 mS/cm^2.) The I–f curves in Fig. 10 indicate the onset of zero-frequency firing as g_K is decreased. We also plot the nullclines for the two-dimensional reduction

$$\dot{V} = -g_{Na} m_\infty^3(V)(1.1 - 1.5n)(V - V_{Na}) - g_K n^4 (V - V_K) - I_L(V) + I_{app}$$

$$\dot{n} = \left(n_\infty(V) - n\right)/\tau_n(V)$$

for $g_K = 20$ and $I_{app} = 1.5$ μA/cm^2, just above rheobase. The orbit shown has 4 Hz frequency.

The (V, n) phase plane of Fig. 10 illustrates the fact that low-frequency firing is obtained because the nullclines are in close proximity in the "ghost" region where the rest state had been for I_{app} just below rheobase. This small regime of close proximity is in contrast to the long "narrow channel" in the model of Rose and Hindmarsh (1985). In that model, the recovery nullcline ($\dot{q} = 0$) has a positive quadratic shape; $q_\infty(V)$ is defined as the sum of $n_\infty^4(V)$ and $b_\infty(V)$. This combination of potassium conductances is based on the CWM axon data and approximates $a_\infty(V)$ as constant. The

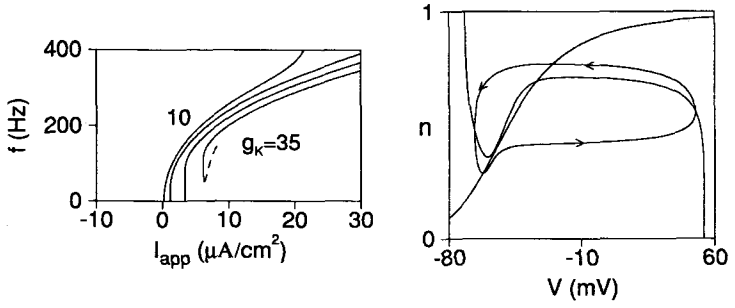

Figure 10. A modified HH system *without* I_A admits zero-frequency firing for certain values of g_K (left). Phase plane (right) for $I_{app} = 1.5$ μA/cm^2 and $g_K = 20$ mS/cm^2 shows stable periodic orbit close to homoclinicity. For slightly larger I_{app}, nullclines intersect at three locations corresponding to non-monotonic $I_{SS}(V)$ for these parameter values.

left branches of the V and q nullclines are nearby each other in the low-voltage region, and over a considerable range of q values, creating a narrow channel through which the solution flows. The nullclines in our example show geometrically that the delayed-rectifier conductance is sufficient for low-frequency firing.

5. Rebound Excitation. So far we have considered steady repetitive firing described by system (3) in response to a maintained and depolarized I_{app} value. Here we focus on the transient aspects of firing. In particular, the rebound spike or spike train that is often elicited when a depolarizing stimulus is applied to a membrane pre-conditioned at a hyperpolarized level. This is an idealization of how timing of excitation-induced spiking might be affected by a long, but finite duration, inhibition. During long-lasting hyperpolarization, I_A may de-inactivate significantly and then be available when the system is released or when a depolarizing input is delivered. Here we assume that the hyperpolarization is long enough for the system to reach a new steady-state (V_h, n_h, b_h). If we step I_{app} to a level above which repetitive firing takes place, I_A is transiently activated but less inactivated than at rest ($b_h > b_0$). This greater I_A conductance slows the initial voltage increase, and thus increases the latency to repetitive firing. For the A_G data set and τ_b small (≈ 1 ms), the latency preceding the first action potential is little affected; it is approximately equal to the interspike interval during steady firing, as shown in Fig. 11A. For the case of τ_b large (≈ 10 ms), however, the latency is prolonged considerably, due to both the increase in τ_b and the ramp effects described in the previous section. For example, suppose we release to $I_{app} = 20\ \mu A/cm^2$ from a hyperpolarized level of $V_h = -90$ mV ($b_h = 0.923$) as shown in Fig. 11B. We can view this trajectory as an orbit in the diagram of Fig. 8B. In this case, $b_A = 9.23$

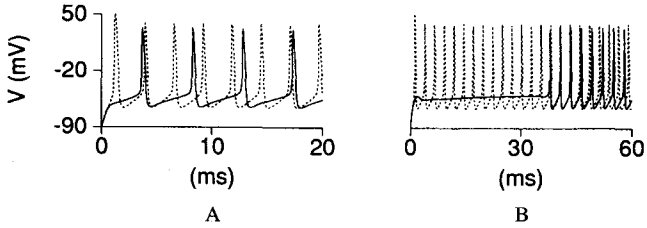

Figure 11. Voltage time course showing latency to firing after depolarizing step of $I_{app} = 20\ \mu A/cm^2$ from pre-hyperpolarization ($V = -90$ mV). These responses of the HHA model (A_G parameter set) show the effects of fast and slow I_A-inactivation: (A) with $\tau_b = 1$ mS and $g_A = 50\ mS/cm^2$ and (B) with $\tau_b = 10$ ms and $g_A = 10\ mS/cm^2$, with I_A present (solid) and blocked (dotted). Note different time scales in (A) and (B).

initially and, upon release, the orbit travels a considerable distance along the steady-state branch of the fast subsystem. If repetitive firing is initiated when $b_A = b_I > b_{SS}$, then the latency, or time it takes b_A to decrease from b_h to b_I, is given by

$$t = \tau_b \ln\left\{\frac{g_A b_\infty(V_{SS}) - b_h}{g_A b_\infty(V_{SS}) - b_I}\right\}. \tag{9}$$

Here we assume that $V = V_{SS}$ is constant along the steady-state branch. For the trajectory in Fig. 11B the latency computed numerically is 40 ms with $b_I = 0.983$. We have no analytical expression for the value of b_I, but the equation (9) does predict that the latency is considerable if τ_b is very large or if $g_A b_\infty(V_{SS}) - b_I = b_{SS} - b_I$ is small.

As illustrated in Fig. 11B when the dynamics of b are slow, a depolarizing I_{app} must last long enough for the model neuron to fire from a pre-hyperpolarized state. An experimental example of this has been described for motoneurons that control the inking response of *Aplysia* (Byrne, 1980). The release of ink occurs selectively in response to long-lasting excitatory input, and I_A is the ionic mechanism attributed to the shift in spiking threshold. Based on our analysis of the underlying bifurcation structure of the HHA model, we predict that a properly timed brief excitatory pulse during the latency phase after application of I_{app} can advance the onset of repetitive firing. In Fig. 12 we plot the latency, or time of first firing, versus the time of the excitatory pulse. Notice that there is a minimum waiting time, below

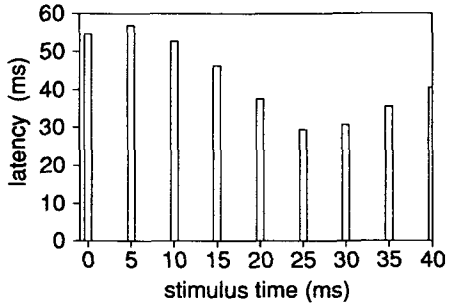

Figure 12. A brief excitatory stimulus can reduce latency to repetitive firing in the HHA model with slowly inactivating generic I_A. Latency (time of first firing) is measured from time zero. Plot shows latency versus time of brief stimulus that is superimposed onto steady current ($I_{app} = 20\ \mu A/cm^2$) initiated at time zero. Brief stimulus: $I_{app} = 1\ \mu A/cm^2$, 0.5 ms duration, initial state: $V = -90$ mV with $g_A = 10$ ms and $\tau_b = 15$ ms. The unperturbed firing time or latency is 55 ms. A minimum latency of 30 ms occurs for a stimulus time of 25 ms. If the stimulus occurs later, the perturbed cell fires instantaneously, i.e. latency equals stimulus time. The amount of latency reduction depends on amplitude and duration of brief pulse.

which the latency cannot be reduced. Given τ_b and b_h, this minimum time is predictable from the bistability in the bifurcation diagram in Fig. 8B. The unstable, periodic solution branch serves as a separatrix to excitation; repetitive firing is initiated if an excitatory pulse of sufficient strength is delivered when $b_A < b_P$. The strength requirement for the pulse is reduced as b_A decreases below b_P; this is obvious since inhibition to excitation is being removed. The minimum time is the time required for b_h to decrease to b_P. Depending on the degree of holding hyperpolarization, b_h may or may not be greater than b_P. If the pre-hyperpolarization is just below rest with $b_h < b_P$, then repetitive firing is initiated as soon as a sufficiently strong pulse is delivered. If τ_b is large, the effect of excitation can be quite significant in advancing activity.

6. Anodal Break Excitation. Anodal break excitation is a special case of rebound excitation when the pre-hyperpolarized system is released to rest. The phenomenon exhibits a threshold which can be defined by viewing a plot of peak voltage, V_{pk}, versus the holding current I_{hold} (Fig. 13A). The stimulus value at which the slope of maximal absolute value occurs is one way the anodal threshold has been defined.

FitzHugh (1976) computed such stimulus–response (I–V_{pk}) curves for the standard HH system without an I_A. He showed that excitation fails given any value for I_{hold} if the temperature is above a critical value of 17.13°C. This is because the (temperature-dependent) rate of I_K activation is increased, allowing n to respond rapidly enough to preclude rebound firing. For temperatures below 17.13°C, if a sufficient amount of n is removed through pre-hyperpolarization, then a full action potential is initiated before n increases significantly.

If I_A is added to the system, the rise of n is influenced by how much I_A slows the approach of V to firing threshold. As a result, for a fixed temperature we also find that rebound excitation is suppressed for large enough g_A, in a manner similar to increases in temperature; that is, the threshold shifts leftward (Fig. 13A). FitzHugh found that the anodal threshold recedes to $-\infty$ as temperature increases. One reason for this is that the stimulus–response curve changes qualitatively; the I–V_{pk} curve becomes more graded. Using the maximal slope definition, there is no temperature at which the threshold disappears; consequently, it goes to $-\infty$ at a critical temperature. This is also the case with the parameter g_A if a slope definition is used. However, we have developed an alternate definition, for which the anodal threshold does not go to $-\infty$. Our definition is in terms of latency rather than V_{pk}, and seems to distinguish better the transitions between sharp and graded responses. Using the fact that the latency (time

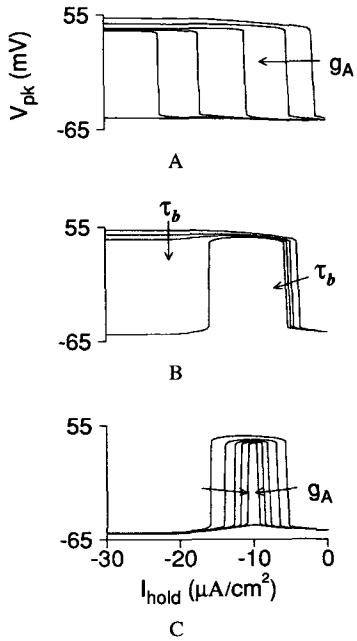

Figure 13. Stimulus–response curves for anodal break excitation. Plots of peak voltage, V_{pk}, after release from pre-hyperpolarization versus holding current I_{hold} show dependence on g_A and τ_b. (A) As g_A increases, the threshold (steep transition in curve; see text for definition) shifts leftward; deeper hyperpolarization is needed to compensate for larger g_A. Here, $\tau_b = 1$ ms; g_A increases from 0 to 50 mS/cm^2, steps of 10. (B) Stimulus regime for rebound response shrinks as inactivation time constant increases. For large enough τ_b, a second threshold, at lower I_{hold}, appears. For I_{hold} very negative, I_A is fully deinactivated, and therefore, if inactivation is very slow, I_A precludes rebound firing. The two thresholds bound a finite window of I_{hold} values release results in rebound excitation. Here, $g_A = 10$ mS/cm^2 and τ_b increases from 1 to 10 ms. (C) The stimulus window for rebound excitation shrinks and disappears as g_A increases ($\tau_b = 10$ ms). Here, $\tau_b = 10$ ms and g_A increases from 10 to 35 mS/cm^2.

to peak) increases monotonically as a critical I_{hold} is approached from either above or below, we search for the maximum latency. For curves as computed in Fig. 13A the sharp threshold behavior disappears for $g_A = 23.8927$ mS/cm^2 at $I_{app} = -36.83$ μA/cm^2. For g_A above this level, the response is considered graded.

Figure 13B shows, as τ_b is increased, the emergence of a second threshold which is lower. In the HHA model whether or not an action potential occurs depends on how V, n and b interact upon release. The total current that inhibits depolarization is $[g_K n^4 + g_A a_\infty^3(V)b](V - V_K)$, but I_K and I_A turn on in different voltage regimes. For small hyperpolarization, $b_h = b_\infty(V_h)$ is negligible because $b_\infty(V)$ is steep with its half-amplitude at

-70 mV. Therefore, there is little increase in I_A conductance upon release, and thus only a slight leftward shift in anodal threshold as τ_b increases. For deep hyperpolarization, the maximal amount of I_A is available to activate upon release ($b_h = 1$). However, b decreases upon release, a process which favors excitation. If this decrease is rapid (τ_b small), then V can escape the inhibition of I_A, and an action potential results. If b decreases slowly (τ_b large), then I_A does not inactivate as V increases. As a result, the action potential is suppressed. If τ_b is not too large, an I_{hold} interval remains in which anodal break excitation occurs (Fig. 13B). The size of this interval depends of g_A. With increasing g_A, the interval decreases to zero, and all anodal excitation is suppressed (Fig. 13C).

7. Discussion. Ever since the work of Connor and Stevens (1971), the presence of potassium A-current has been associated with extending a neuron's range of firing frequencies, especially at the lower end to arbitrarily slow rates. Numerous other transient potassium currents have been found subsequently, and their describing parameter values span a large range. These currents inactivate at depolarized levels and so their primary effects are on behavior in the subthreshold voltage range, to increase interspike intervals during repetitive firing and to increase the latency before firing when stimulated from hyperpolarized holding states. During firing, if there is substantial post-spike hyperpolarization, then I_A may recover adequately to delay the next spike. In some cases, I_A may even play a role to help repolarize the membrane. The size of these effects depends on several I_A parameters, notably on the inactivation time constant τ_b.

In order to systematically explore how I_A effects input–output properties we have defined two A-current parameter sets: A_G, for a "generic" A-current that typifies much of the voltage-clamp data in the literature, and A_C, for I_A from Conner *et al.* (1977) whose activation parameter values differ considerably from those of most I_As. With the intent of avoiding extraneous details, we incorporated I_A into a minimal action potential model, a two-variable reduction of the standard Hodgkin–Huxley (HH) equations. Our analysis for the case of Connor-like parameters elucidated the mechanism underlying low-frequency firing: the emergence of periodic behavior via bifurcation of a homoclinic solution (infinite period) at a saddle-node of steady states. As the maximal conductance g_A of I_A is decreased, the minimum firing rate increases from zero. The onset of repetitive firing changes from a homoclinic to a subcritical Hopf bifurcation, and thus when $g_A = 0$ the onset is as that in the classical HH model. In contrast, for our generic A-current (A_G parameter set), we did not find very low firing rates;

instead, the onset of firing occurs with non-zero frequency over a large range of g_A.

Gerber and Jakobsson (1993) have also explored the effects of Connor's A-current on firing behavior. They confirmed the frequency reductions and noted that they were limited to a narrow interval of stimulus values near threshold. Our work provides the mathematical explanation in terms of bifurcation theory for the frequency reduction. We also clarified that an important biophysical correlate for arbitrarily low firing rates is the necessity that the membrane have an N-shaped steady-state, current–voltage relation. The N-shape condition can be realized, of course, by numerous combinations of ionic currents, but it does not require an A-current. Indeed, we have verified that our reduced HH model with $g_A = 0$ and with slightly modified parameters for I_{Na} and I_K can produce low firing rates (see also Rinzel and Ermentrout, 1989).

We also found new behaviors mediated by I_A when its inactivation rate is slow. Periodic bursting arises in certain stimulus regimes for our generic I_A. During a burst's spiking phase, I_A slowly de-inactivates, recovering a little during the hyperpolarization that follows each spike. When sufficiently de-inactivated, I_A terminates the burst. Then during the interburst phase, inactivation proceeds slowly until the membrane can begin spiking again. Modulating the A-current parameters, particularly the rate of inactivation, can significantly change burst duration, and thus can play role in regulating synaptic transmission. Recently, Wang (1993) reported that clusters of Na^+ spikes could provide a possible means for *transient* synchrony in a network of neurons. Likewise in his model, a slowly inactivating transient potassium current underlies spike bursting (with interburst behavior distinguished by subthreshold oscillations). Viewing our generic A-current as representation of a family of such potassium currents, we offer a qualitative explanation for this burst behavior. Mathematically, the mechanism depends on a subcritical Hopf bifurcation for the fast spike-generating subsystem as described by Rinzel (1987) for a FitzHugh–Nagumo-like model.

The A-current has been implicated in reducing the excitability in neurons not only by shifting the stimulus threshold for repetitive firing, but also by delaying its onset after initiation of a sustained depolarizing input. If a cell is pre-conditioned in a hyperpolarized voltage regime where I_A inactivation is removed, repetitive firing evoked by a depolarizing stimulus is delayed until I_A inactivates. The delay is quite considerable for slow I_A inactivation. Gerber and Jakobsson (1993) emphasize this functional role of I_A by showing the relationship between the inactivation time constant and the initial delay. What we found is that the onset of repetitive firing can be advanced by a brief excitatory pulse. Beyond a critical time during the latency phase, repetitive firing can be evoked prematurely and immediately.

Thus while the neuron's overall responsiveness to excitation may be reduced by I_A, it may remain responsive to more selective (i.e. well timed) brief synaptic events.

Storm (1988) has reported remarkably long delays (10 sec) to firing in rat hippocampal neurons where the transient K^+ current elicited by a step from hyperpolarization consisted of two components: a fast I_A and a slowly inactivating current called I_D. Apparently, I_A is too fast to account for most of the delay, yet I_D, or "delay current," is characteristic of our generic I_A: rapid, subthreshold activation and slow inactivation. Storm suggests that these properties may mediate slow temporal integration of repeated depolarizing inputs. We have shown that a single depolarizing pulse failed to depolarize the cell to spike threshold unless properly timed; that is, unless inactivation has decreased sufficiently. Based on this, we would predict that given sufficient pre-hyperpolarization, repeated inputs (with slow recovery of inactivation between pulses) could result in a slow voltage buildup toward threshold. This delay of excitation in the presence of depolarizing events is an important mechanism in certain neurons, and those elements characteristic of our slow generic I_A seem to play an important role.

APPENDIX

Parameters and Functions for the Hodgkin–Huxley Equations.

$$\alpha_m(V) = 0.1(V + 35 - \sigma_m)/(1.0 - \exp[-0.1(V + 35 - \sigma_m)])$$

$$\beta_m(V) = 4\exp[-0.05(V + 60 - \sigma_m)]$$

$$\alpha_h(V) = 0.07\exp[-(V + 60 - \sigma_h)]$$

$$\beta_h(V) = 1/(\exp[-0.1(V + 30 - \sigma_h)] + 1)$$

$$\alpha_n(V) = 0.01(V + 50 - \sigma_n)/(1.0 - \exp[-0.1(V + 50 - \sigma_n)])$$

$$\beta_n(V) = 0.125\exp[-0.0125(V + 60 - \sigma_n)]$$

$$m_\infty(V) = \alpha_m(V)/[\alpha_m(V) + \beta_m(V)]; \quad \tau_m(V) = t_m/(\alpha_m(V) + \beta_m(V))$$

$$h_\infty(V) = \alpha_h(V)/[\alpha_h(V) + \beta_h(V)]; \quad \tau_h(V) = t_h/(\alpha_h(V) + \beta_h(V))$$

$$n_\infty(V) = \alpha_n(V)/[\alpha_n(V) + \beta_n(V)]; \quad \tau_n(V) = t_n/(\alpha_n(V) + \beta_n(V))$$

$$\phi = 3^{(\text{Temp}-6.3)/10} \quad \text{and} \quad t_i = 1/\phi,\ i = m, h, n.$$

Adjustments to the Hodgkin–Huxley equations by Connor *et al.* are given by $\sigma_m = 5.3$, $\sigma_h = 12$ and $\sigma_n = 4.3$, as well as $t_n = 2/\phi$, where ϕ is the temperature adjustment factor. $g_{Na} = 120$ and g_K is reduced from 36 to 20.

REFERENCES

Awiszus. F. 1992. Reduction of a Hodgkin–Huxley-type model for a mammalian neuron at body temperature. *Biol. Cybern.* **67**, 427–432.

Baer, S. M., T. Erneux and J. Rinzel. 1989. The slow passage through a Hopf-bifurcation: delay, memory effects and resonance. *SIAM J. Appl. Math.* **49**, 55–71.

Bargas, J., E. Galarraga and J. Aceves. 1989. An early outward conductance modulates the firing latency and frequency of neostriatal neurons of the rat brain. *Exp. Brain Res.* **75**, 146–156.

Bogdanov, R. I. 1975. Versal deformations of a singular point on the plane in the case of zero eigenvalues. *Funct. Anal. Appl.* **9**, 144–145.

Buchholtz, F., J. Golowasch, I. R. Epstein and E. Marder. 1992. Mathematical model of an identified stomatiogastric ganglion neuron. *J. Neurophysiol.* **67**, 332–340.

Byrne, J. H. 1980. Quantitative aspects of ionic conductance mechanisms of contributing to firing patterns of motor cells mediating inking behavior in *aplysia californía*. *J. Neurophysiol.* **43**, 651–668.

Connor, J. A. and C. F. Stevens. 1971. Prediction of repetitive firing behavior from voltage-clamp data on an isolated neurone soma. *J. Physiol. Lond.* **214**, 31–53.

Connor, J. A., D. Walter and R. McKown. 1977. Neural repetitive firing: modifications of the Hodgkin–Huxley axon suggested by experimental results from crustacean axons. *Biophys. J.* **18**, 81–102.

Dekin, M. S. and P. A. Getting. 1987. In vitro characterization of neurons in the ventral part of the nucleus tractus solitarius. III. ionic basis for repetitive firing patterns. *J. Neurophysiol.* **58**, 215–229.

Dodge, F. A. 1972. On the transduction of visual, mechanical, and chemical stimuli. *Int. J. Neurosc.* **3**, 5–14.

Doedel, E. J. 1981. AUTO: A program for the automatic bifurcation analysis of autonomous systems. *Congr. Numer.* **30**, 265–284.

FitzHugh, R. 1976. Anodal excitation in the Hodgkin–Huxley nerve model. *Biophy. J.* **16**, 209–226.

Gerber, B. and E. Jakobsson. 1993. The functional significance of the A-current. *Biol. Cybernetics.* **70**, 109–114.

Getting, P. 1983. Mechanisms of pattern generating underlying swimming in *Tritonia*. III. intrinsic and synaptic mechanisms for delayed excitation. *J. Neurophysiol.* **49**, 1036–1050.

Golowasch, J. and E. Marder. 1992. Ionic currents of the lateral pyloric neuron of the stomatogastric ganglion of the crab. *J. Neurophysiol.* **66**, 318–331.

Graubard, K. and D. K. Hartline. 1991. Voltage clamp analysis of intact stomatogastric neurons. *Brain Res.* **557**, 241–254.

Guckenheimer, J., S. Gueron and R. M. Harris-Warrick. 1992. Mapping the dynamics of a bursting neuron. *Phil. Trans. Roy. Soc. Lond. Ser. B* **341**, 345–359.

Hassard, B. D. and L. J. Shiau. 1991. Degenerate Hopf bifurcation and isolated periodic solutions of the Hodgkin–Huxley model with varying sodium ion concentration. *J. Theor. Biol.* **148**, 157–173.

Hodgkin, A. L. and A. F. Huxley. 1952. A quantitative description of membrane current and its application to conduction in nerve. *J. Physiol. Lond.* **117**, 500–544.

Huguenard, J. R. and D. A. McCormick. 1992. Simulation of the currents involved in rhythmic oscillations in thalamic relay neurons. *J. Neurophysiol.* **68**, 1373–1383.

Kaczmarek, L. K. and F. Strumwasser. 1984. A voltage-clamp analysis of currents underlying cyclic amp-induced membrane modulation in isolated peptidergic neurons of *Aplysia*. *J. Neurophysiol.* **52**, 340–349.

Kernell, D. and H. Sjoholm. 1973. Repetitive impulse firing: comparison between neurone models based on voltage clamp equations and spinal motoneurones. *Acta Physiol. Scand.* **87**, 40–56.

Labouriau, I. S. 1989. Degenerate Hopf bifurcation and nerve impulse. Part II. *SIAM J. Math. Anal.* **20**, 1–12.

McCormick, D. A. 1991. Functional properties of a slowly inactivating potassium current in guinea pig dorsal lateral geniculate relay neurons. *J. Neurophysiol.* **66**, 1176–1189.

Neher, E. 1971. Two fast transient current components during voltage clamp on snail neurons. *J. Gen. Physiol.* **58**, 36–53.

Rinzel, J. 1978. On repetitive activity in nerve. *Federation Proc.* **37**, 2793–2802.

Rinzel, J. 1985. Excitation dynamics: insights from simplified membrane models. *Federation Proc.* **44**, 2944–2946.

Rinzel J. 1987. A formal classification of bursting mechanisms in excitable systems. In *Mathematical Topics in Population Biology Morphogensis and Neurosciences. Lecture Notes in Biomathematics* T. E. and M. Yamaguti (Eds), Vol. 71, pp. 267–281. New York: Springer-Verlag.

Rinzel, J. and G. B. Ermentrout. 1989. Analysis of neural excitability and oscillations. In *Methods in Neuronal Modeling: From Synapses to Networks* C. Koch and I. Seger (Eds), pp. 135–169. Cambridge MA: MIT Press.

Rogawski, M. A. 1985. The A-current: how ubiquitous a feature of excitable cells is it? *Trends Neurosci.* **8**, 214–219.

Rose, R. M. and J. L. Hindmarsh. 1985. A model of a thalamic neuron. *Proc. Roy. Soc. Lond. Ser. B* **225**, 161–193.

Shapiro, B. I. and F. K. Lenherr. 1972. Increased modulation and linearity to response to constant current stimulus. *Biophys. J.* **12**, 1145–1158.

Storm, J. F. 1988. Temporal integration by a slowly inactivating K^+ current in hippocampal neurons. *Nature* **336**, 379–381.

Surmeier, D. J., J. Bargas. and S. T. Kitai. 1988. Voltage-clamp analysis of a transient potassium current in rat neostriatal neurons. *Brain Res.* **473**, 187–192.

Surmeier, D. J., J. Bargus. and S. T. Kitai. 1989. Two types of A-current differing in voltage-dependence are expressed by neurons of the rat neostriatum. *Neurosci. Lett.* **103**, 331–337.

Takens, F. 1974. Singularities of vector fields. *Publ. Math. IHES* **43**, 47–100.

Thompson, S. 1977. Three pharmacologically distinct potassium channels in molluscan neurones. *J. Physiol.* **265**, 465–488.

Thompson, S. 1982. Aminopyridine block of transient potassium current. *J. Gen. Physiol.* **80**, 1–18.

Wang, X. J. 1993. Ionic basis for intrinsic 40 Hz neuronal oscillations. *NeuroReport* **5**, 221–224.

Williams, J. T., R. A. North, S. A. Shefner, S. Nishi and T. M. Egan. 1984. Membrane properties of rat locus coeruleus neurons. *Neuroscience* **13**, 137–156.

Received 29 October 1994
Revised version accepted 25 May 1995